Loss Distribution in an Electric Vehicle Traction Chain using a Cascaded H-Bridge Inverter with Integrated Battery

Gaël Pongnot, Clément Mayet, Denis Labrousse

pcim
EUROPE

Loss Distribution in an Electric Vehicle Traction Chain using a Cascaded H-Bridge Inverter with Integrated Battery

Gaël Pongnot[1], Clément Mayet[1,2], Denis Labrousse[1,2]

[1] SATIE, Université Paris-Saclay, ENS Paris-Saclay, CNRS, F-91190, Gif-sur-Yvette, France
[2] SATIE, Le Cnam, CNRS, F-75003, Paris, France, HESAM Université

Corresponding author: Gaël Pongnot, gael.pongnot@ens-paris-saclay.fr
Speaker: Gaël Pongnot, gael.pongnot@ens-paris-saclay.fr

Abstract

This paper attempts to determine the sources of loss of a cascaded H-bridge inverter with integrated batteries (CHB-IB) when used to supply an electric vehicle traction machine. An Energetic Macroscopic Representation (EMR) is performed to model the sources of losses and to simulate the behavior of the different system elements. Waveforms illustrate critical operating points, including loss models for each element. Simulation results are presented as a function of the torque and speed of the machine to identify trends. An analysis of these results is proposed, and the primary source of losses is highlighted.

1 Introduction

Electric vehicles (battery-powered and plug-in hybrids) represent 17% of sales in 2021 in Europe [1]. However, deep market penetration requires battery electric vehicles (BEV) to have an acceptable range at a reasonable cost. Therefore, research focuses on increasing batteries' energy density and improving the energy efficiency of the entire power train. Furthermore, the increase in the share of intermittent energies on the electrical grid leads to the need for increased energy storage capacities. BEVs can contribute to this development through Vehicle to Grid (V2G) technology.

In this context, a structure called a cascaded H-bridge inverter with integrated battery (CHB-IB) was proposed in the late twenty century to replace the conventional traction system of BEVs (Fig. 1) [2]. Numerous studies have been conducted since then [3]–[8]. This structure is now seriously considered by some car manufacturers like Stellantis [9].

This structure combines the functionalities of the battery pack, traction inverter, and charger. Battery cells are used as storage elements of a cascaded H-bridge inverter, thus replacing the traditional capacitors. This combination of batteries and power electronics creates a modular structure capable of generating a variable amplitude voltage at a variable frequency to control and supply the traction machine. Previous papers have described this structure, and its control [4], [8]. Moreover, it is also possible to connect this converter to a single-phase or three-phase network, or a continuous fast charging station, with some reconfiguration.

This modular multilevel converter offers a large number of degrees of freedom. Various controls can be offered, including nearest level control (NLC) which does not use PWM. This control, preferred in this study, reduces the global losses of power electronic devices by limiting the number of switching. Thus, compared to conventional topologies, significant overall efficiency improvements are expected when using a CHB-IB [6].

This paper aims to estimate the efficiency of a CHB-IB associated with a permanent magnet synchronous traction machine (PMSM) for several torque and speed loads. Section 2 presents the CHB-IB: architecture and control. Section 3 details the loss models, including several sources of losses. Finally, the simulation results are presented and analyzed in section 4, allowing estimation of the losses and efficiencies separately for the batteries, the H-bridge converters, and the PMSM.

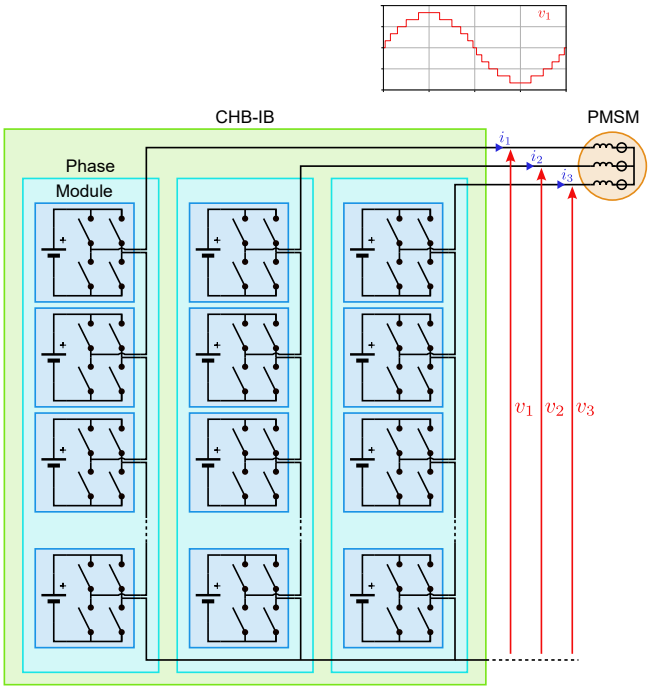

Fig. 1: CHB-IB Traction Chain Topology

2 Description and Control of CHB

The CHB-IB uses three phases to power the traction machine, as presented by Fig. 1. Each phase p consists of M modules connected in series, typically 24. A module, indexed by m, is formed of an H-bridge associated with a battery. Each switch of the H-bridges is made of two paralleled MOSFETs 40 V 500 A. Batteries consist of four Li-ion cells connected in series. In total, 288 cells are on board, equivalent to current BEVs.

The output voltage of each module can take three values, consequences of the four possible states of an H-bridge: $+v_{p,m\,\mathrm{bat}}$, 0 or $-v_{p,m\,\mathrm{bat}}$. Equation (1) reflects that the phase voltage v_p is the sum of the voltages of modules $v_{p,m}$. Since NLC is used, PWM is not allowed, and the phase voltage has a typical waveform with voltage steps (Fig. 1), similar to a quantization of the voltage.

$$v_p = \sum_{m=1}^{M} v_{p,m} \tag{1}$$

Figure 2 represents the traction train using an Energetic Macroscopic Representation (EMR) [10]. The control signals $u_{p,m,b}$ of the $6M$ commutation cells (CC) are synthesized from a phase voltage reference $v_{p\,\mathrm{ref}}$ by model inversion [8], [11].

3 Energetic Loss-Oriented Model

In this paper, the CHB-IB is coupled to a PMSM, which is characteristic of its use in a BEV. The machine reduces the study quantities to two mechanical quantities: torque and speed. Indeed, the control strategy of the machine makes the additional quantities non-independent. The machine is considered with smooth poles, so the chosen control maximizes the torque.

Each subsystem of the traction chain has its own behavior; the first step is to model them. It will then be possible to dissociate the losses according to their origin: battery, converter, and machine.

3.1 Synchronous Machine

The considered PMSM is assumed not to be saturated. Table 1 summarizes its characteristics. A stator resistance R_s models the copper losses, while a constant electromagnetic efficiency coefficient η_em models the iron losses.

Equations (2) and (3) present its operation in the Park's reference frame. The vectors and matrices are in bold font, and $\mathbf{e_{dq0}}$ corresponds to the emf.

$$T = \eta_\mathrm{em} n_\mathrm{p} \psi_\mathrm{d} i_\mathrm{q} \tag{2}$$

$$\mathbf{v_{dq0}} = R_\mathrm{s}\mathbf{i_{dq0}} + \mathbf{L_{dq0}}\frac{\mathrm{d}\mathbf{i_{dq0}}}{\mathrm{d}t} + \mathbf{e_{dq0}} \tag{3}$$

Quantity	Symbol	Value	Unit
Max Power	P_max	60	kW
Max Speed	N_max	18 000	rpm
Max Current	I_max	500	A
Max Torque	T_max	100	N m
Stator Resistance	R_s	8.5	mΩ
D-axis Inductance	L_d	366	µH
Q-axis Inductance	L_q	366	µH
D-axis Flux	ψ_d	40	mWb
Pole pairs	n_p	4	
EM efficiency	η_em	99	%

Tab. 1: PMSM Parameters

3.2 Converter

The H-bridge converters consist of two arms based on low-voltage Si MOSFETs. These four transistors induce conduction losses and switching losses. Table 2 gives their characteristics.

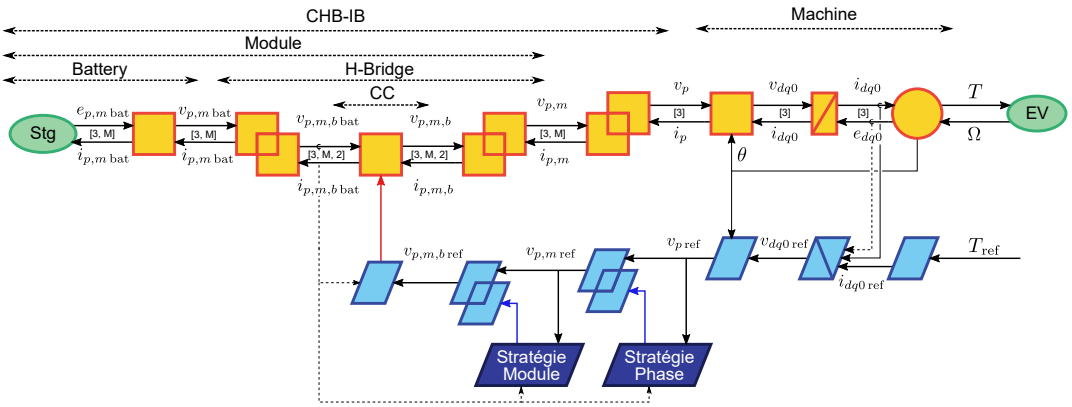

Fig. 2: Energetic Macroscopic Representation of a CHB-IB Traction Chain

A MOSFET transistor in the on state behaves like a resistor, noted R_{on}. It induces a voltage drop in the transistor, modeled by Eq. (4). This resistance depends strongly on the temperature, which introduces a thermal coupling that complicates the calculation of conduction losses. Here, the operating temperature is considered constant and equal to a targeted steady state of 80 °C.

The switching losses are difficult to determine for MOSFETs. This paper uses a model based on the work of Christen and Biela [12]. It estimates these losses by considering the parameters of the technical documentation of the component. The energy dissipated at each switching is calculated according to an analytical model and then introduced in the simulation as an additional current $i_{p,m,b\,\text{sw}}$ in the battery during a fixed time, Eq. (5).

$$v_{p,m,b} = u_{p,m,b} v_{p,m,b\,\text{bat}} - R_{\text{on}} i_{p,m,b} \tag{4}$$

$$i_{p,m,b\,\text{bat}} = u_{p,m,b} i_{p,m,b} + i_{p,m,b\,\text{sw}} \tag{5}$$

Quantity	Symbol	Value	Unit
Max Voltage	V_{max}	40	V
Max Current	I_{max}	500	A
Resistance (80 °C)	R_{on}	0.55	mΩ

Tab. 2: MOSFET Parameters

3.3 Battery

Li-ion batteries can be described using complex electrokinetic models or equivalent Randles models. Previous research has shown that these dynamics are essential in the case of a CHB for calculating losses due to low-frequency current ripples [7].

However, in this paper, a static model is considered to simplify the model and decrease the computation time. Equation (6) shows the introduction of a resistive component R_{bat}. This choice leads to overestimating the losses that [7] estimates at 20% compared to experimental results. Table 3 provides the characteristic data of the battery.

$$v_{p,m\,\text{bat}} = e_{p,m\,\text{bat}} - R_{\text{bat}} i_{p,m\,\text{bat}} \tag{6}$$

Quantity	Symbol	Value	Unit
Max Voltage	e_{max}	4	V
Min Voltage	e_{min}	3	V
Op. Voltage	e_{op}	4	V
Num. serial cells	n_{c}	4	
Resistance	R_{bat}	3.5	mΩ

Tab. 3: Battery Parameters

3.4 Control

The machine has a dedicated adaptive PI controller to control the torque. This controller is tuned as a pole compensator with a response time equal to one electrical period. Thus, the speed of the machine becomes an input variable of the controller. This control is achievable because the speed varies slowly compared to electrical quantities.

The control of the CHB-IB is performed by model inversion, as detailed in [8]. An active state-of-charge balancing strategy for the battery cells is implemented. This control strategy is not studied in this paper but justifies considering battery voltages to be identical for all modules: $e_{p,m\,\text{bat}} = e_{\text{op}}$.

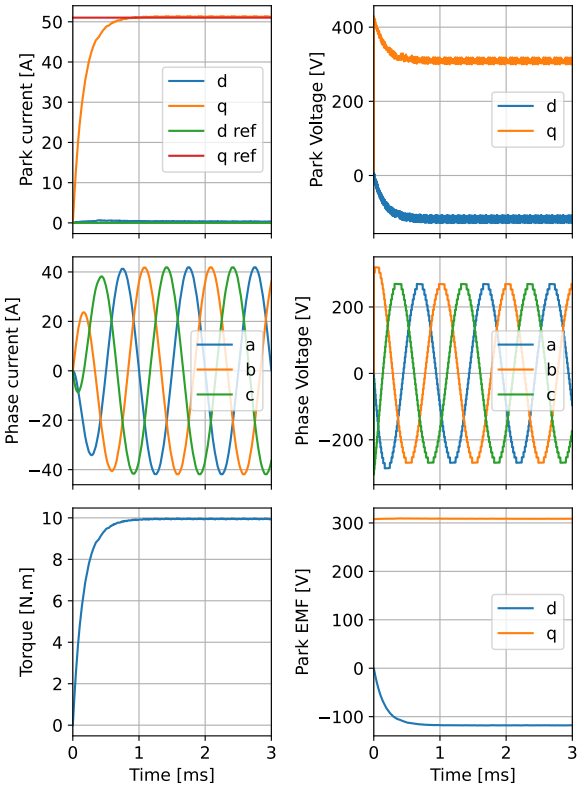

Fig. 3: High speed OP ($T = 10\,\mathrm{N\,m}$, $N = 15\,000\,\mathrm{rpm}$)

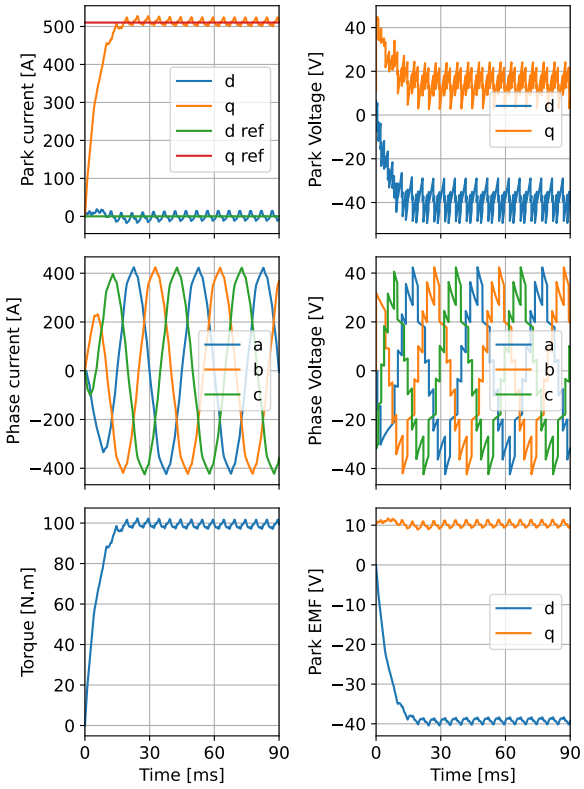

Fig. 4: High torque OP ($T = 100\,\mathrm{N\,m}$, $N = 500\,\mathrm{rpm}$)

4 Performance Analysis

4.1 Waveform

This model allows the simulation of different operating points (OP), as shown in Figs. 3 and 4. The simulation lasts between one and five minutes. The waveforms illustrate the voltage level modulation.

At high speed (Fig. 3), the output voltage is high, so many levels are required. The voltage is quasi-sinusoidal, a little ripple visible in the dq0 space (Park transformation). In this case, the current is close to the perfect sinusoid, inducing a tiny current ripple.

On the contrary, at low speed, few levels are needed, which induces a coarser quantization of the reference sinusoid and, thus, a higher ripple. Moreover, Fig. 4 shows a high-current operation, which induces a significant voltage drop. The voltage steps are no longer constant with time.

In a classical structure, the current ripple is related to the switching frequency of the inverter. Whereas, with the CHB structure, this ripple is a consequence of the number of voltage levels used. The current ripple directly creates a torque ripple. Thus, the estimation of the torque ripple will be necessary for subsequent studies to judge the quality of the waveforms produced by the CHB.

4.2 Energy Balance

The simulation of a large number of operating points enables the mapping of the efficiency in the torque-speed field. The first step defines the interest quantities to study these power flows. Equations (7) to (10) define four powers: P_{SM} being the mechanical power at the output of the machine, P_{CHB} the power at the output of the CHB, P_{bat} the power at the output of the battery and P_{stg} the usable internal power of the battery.

$$P_{\mathrm{SM}} = T\Omega = \tfrac{30}{\pi} TN \tag{7}$$

$$P_{\mathrm{CHB}} = \sum_{p=1}^{3} v_p i_p = v_{\mathrm{d}} i_{\mathrm{d}} + v_{\mathrm{q}} i_{\mathrm{q}} + v_0 i_0 \tag{8}$$

$$P_{\mathrm{bat}} = \sum_{p=1}^{3} \sum_{m=1}^{M} v_{p,m\,\mathrm{bat}} i_{p,m\,\mathrm{bat}} \tag{9}$$

$$P_{\mathrm{stg}} = \sum_{p=1}^{3} \sum_{m=1}^{M} e_{p,m\,\mathrm{bat}} i_{p,m\,\mathrm{bat}} \tag{10}$$

Based on these different powers, Eqs. (11) to (13) define efficiencies for the three components of the system: battery, CHB and PMSM. Then, global efficiency is defined by Eq. (14).

$$\eta_{\mathrm{SM}} = \left(\frac{P_{\mathrm{SM}}}{P_{\mathrm{CHB}}} \right)^{\frac{P_{\mathrm{SM}}}{|P_{\mathrm{SM}}|}} \tag{11}$$

$$\eta_{\mathrm{CHB}} = \left(\frac{P_{\mathrm{CHB}}}{P_{\mathrm{bat}}} \right)^{\frac{P_{\mathrm{CHB}}}{|P_{\mathrm{CHB}}|}} \tag{12}$$

$$\eta_{\mathrm{bat}} = \left(\frac{P_{\mathrm{bat}}}{P_{\mathrm{stg}}} \right)^{\frac{P_{\mathrm{bat}}}{|P_{\mathrm{bat}}|}} \tag{13}$$

$$\eta = \left(\frac{P_{\mathrm{SM}}}{P_{\mathrm{stg}}} \right)^{\frac{P_{\mathrm{SM}}}{|P_{\mathrm{SM}}|}} \tag{14}$$

Figure 5 shows the overall system's efficiency in the torque-speed field. This representation is obtained by simulating numerous operating points for several days. The red line represents the nominal limits of the machine, and the white space is an area inaccessible by the system.

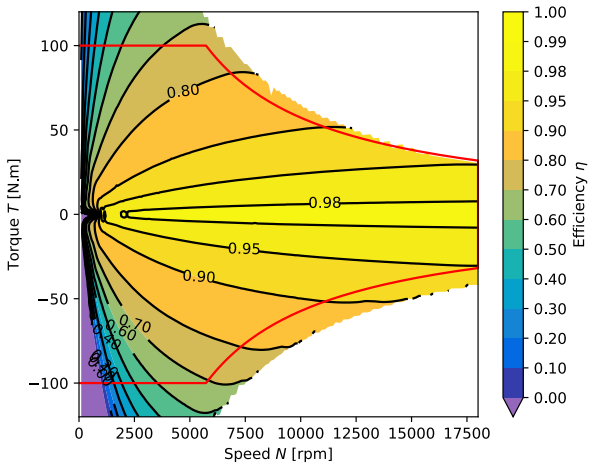

Fig. 5: Total Efficiency

Three situations can be distinguished: driving, regenerative braking, and active braking. The first two cases are typical operations, with power flowing from the battery to the machine and vice versa, as shown in the Sankey diagrams Figs. 6 and 7. In these areas, efficiency ranges from 0 to 99 %, with the maximum being reached for high speed and low torque (Fig. 3). High-torque operation suffers from a degraded efficiency at equivalent power, and low speed strongly degrades efficiency (Fig. 4).

Negative efficiency situations exist. They correspond to an active braking situation. In these configurations, the vehicle slows down using power from the batteries. All the power is then dissipated in the battery, the CHB, or the machine ; Figure 8 illustrates an operation where the power goes into the CHB. It decreases autonomy and creates unnecessary heating. The use of mechanical braking can avoid these active braking situations.

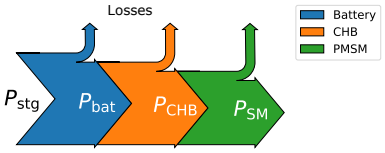

Fig. 6: Driving Power Flow

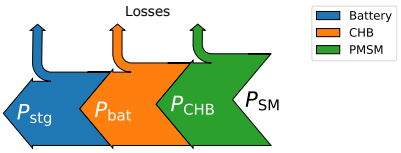

Fig. 7: Regenerative Braking Power Flow

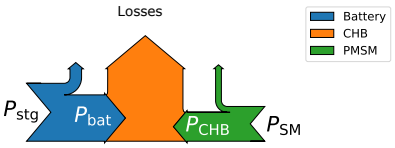

Fig. 8: Active Braking Power Flow

Figures 9 to 11 show the efficiencies of the different elements. Some trends are familiar with Fig. 5. In particular, the efficiency of the machine and the CHB strongly depends on the power distribution between torque and speed. These simulation results show that the losses originate mainly from conduction losses. The situations of high currents are thus unfavorable. These configurations of high current correspond to high torque, hence this aspect. On the other side, the efficiency of the batteries is almost independent of the speed above 2000 rpm. Indeed, the equivalent resistance of the battery is proportional to the number of active modules and, thus, to the output voltage of the cascaded H-bridge converter.

Figure 12 presents the element that dissipates the most energy according to the operating point. The observed areas are easily explained. The equivalent resistance of the CHB is constant because $2M$ transistors are always conducting, while the equivalent resistance of the battery is proportional

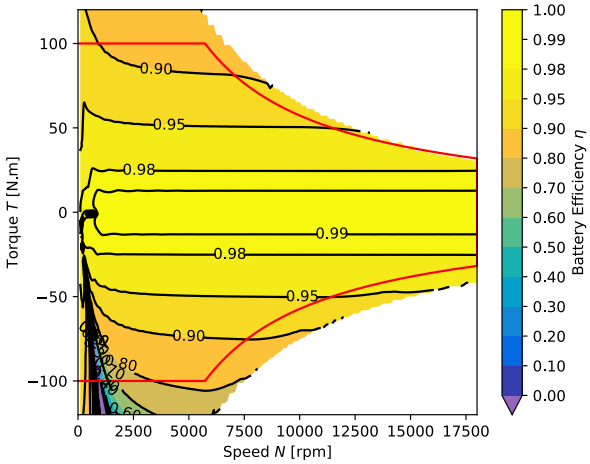

Fig. 9: Battery Efficiency

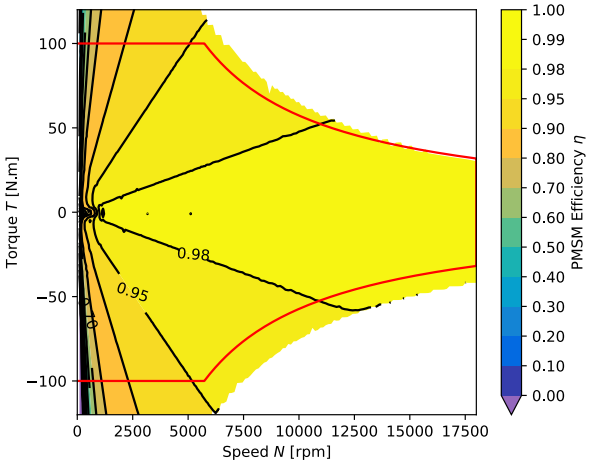

Fig. 11: PMSM Efficiency

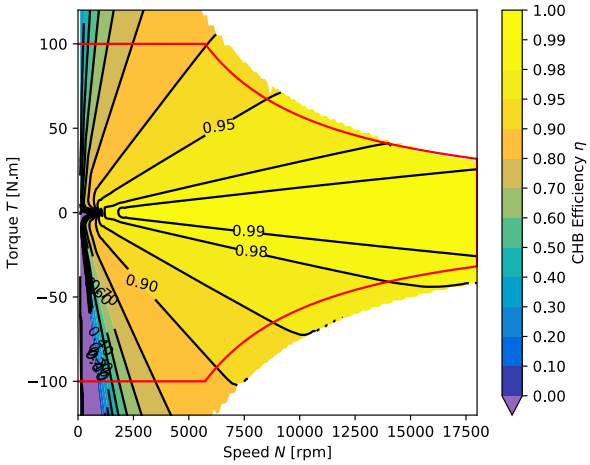

Fig. 10: CHB Efficiency

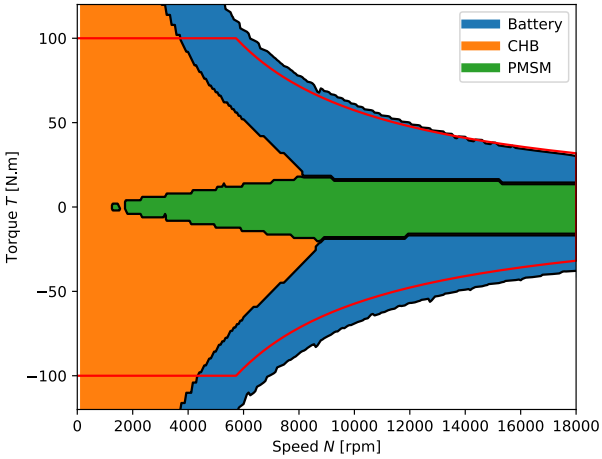

Fig. 12: Maximum Losses Localisation

to the voltage, thus, to the speed. Consequently, the losses in the CHB are predominant at low speeds because the resistance of the batteries is low. When the required torque is low, little current is needed. Then, the electromagnetic efficiency of the machine becomes limiting: the machine is the primary source of losses at low torque.

5 Conclusion

Cascaded H-bridge multilevel inverters are a serious alternative to standard two-level inverters for electric drive chains. Simulations conducted in this paper aimed to estimate the efficiency of this structure in an electric drive in the torque-speed field using a Nearest-Level Control. The losses are separated between the battery, the CHB, and the PMSM. The simulations are conducted using analytical loss models. The Energetic Macroscopic Representation organizes the different models according to the physical energy properties.

Simulation results show that losses significantly impact the generated waveforms, especially for high-torque operating points. Moreover, low-voltage operations induce a significant torque ripple. Further studies should focus on this ripple and its consequences regarding mechanical vibrations and user comfort.

Exploration of the torque-speed fields demonstrates a high efficiency for high-speed operations. Furthermore, the origins of the losses are demonstrated and analyzed. In addition, some atypical points are highlighted, such as active braking,

which should be avoided. Finally, the primary source of loss is identified according to the torque-speed operation point.

This paper is a crucial step for the subsequent studies, which can focus on comparing competing architectures (Si and SiC inverters) and controls for different operating points and driving cycles.

6 Acknowledgments

This paper has been achieved within IBIS project, funded by ADEME (*Agence de l'environnement et de la maîtrise de l'énergie*) through "le Programme d'investissements d'avenir (PIA)".

References

[1] L. Paoli, A. Dasgupta, and S. McBain, "Electric Vehicles," IEA, Paris, 2022.

[2] L. Tolbert, F. Z. Peng, and T. Habetler, "Multilevel converters for large electric drives," *IEEE Transactions on Industry Applications*, vol. 35, no. 1, pp. 36–44, Jan. 1999. DOI: 10.1109/28.740843.

[3] L. Tolbert, F. Z. Peng, T. Cunnyngham, and J. Chiasson, "Charge balance control schemes for cascade multilevel converter in hybrid electric vehicles," *IEEE Transactions on Industrial Electronics*, vol. 49, no. 5, pp. 1058–1064, Oct. 2002. DOI: 10.1109/TIE.2002.803213.

[4] L. Mathe, P. Dan Burlacu, E. Schaltz, and R. Teodorescu, "Battery pack state of charge balancing algorithm for cascaded H-Bridge multilevel converters," in *2016 IEEE 16th International Conference on Environment and Electrical Engineering (EEEIC)*, Jun. 2016, pp. 1–6. DOI: 10.1109/EEEIC.2016.7555737.

[5] M. Quraan, T. Yeo, and P. Tricoli, "Design and Control of Modular Multilevel Converters for Battery Electric Vehicles," *IEEE Transactions on Power Electronics*, vol. 31, no. 1, pp. 507–517, Jan. 2016. DOI: 10.1109/TPEL.2015.2408435.

[6] F. Chang, O. Ilina, M. Lienkamp, and L. Voss, "Improving the Overall Efficiency of Automotive Inverters Using a Multilevel Converter Composed of Low Voltage Si mosfets," *IEEE Transactions on Power Electronics*, vol. 34, no. 4, pp. 3586–3602, Apr. 2019. DOI: 10.1109/TPEL.2018.2854756.

[7] O. Theliander, A. Kersten, M. Kuder, W. Han, E. A. Grunditz, and T. Thiringer, "Battery Modeling and Parameter Extraction for Drive Cycle Loss Evaluation of a Modular Battery System for Vehicles Based on a Cascaded H-Bridge Multilevel Inverter," *IEEE Transactions on Industry Applications*, vol. 56, no. 6, pp. 6968–6977, Nov. 2020. DOI: 10.1109/TIA.2020.3026662.

[8] C. Mayet, D. Labrousse, R. Bkekri, F. Roy, and G. Pongnot, "Energetic Macroscopic Representation and Inversion-Based Control of a Multi-Level Inverter with Integrated Battery for Electric Vehicles," in *2021 IEEE Vehicle Power and Propulsion Conference (VPPC)*, Gijon, Spain: IEEE, Oct. 2021, pp. 1–6. DOI: 10.1109/VPPC53923.2021.9699228.

[9] F. Roy and B. Revol, "Batterie à groupes de cellule(s) de stockage associés respectivement à des modules de conversion, pour la fourniture de tensions de types différents," French pat. 3063188A1, Aug. 24, 2018.

[10] A. Bouscayrol and B. Lemaire-Semail, "Energetic macroscopic representation and inversion-based control," in *Encyclopedia of Electrical and Electronic Power Engineering*, J. García, Ed., Oxford: Elsevier, Jan. 1, 2023, pp. 365–375. DOI: 10.1016/B978-0-12-821204-2.00117-3.

[11] W. Lhomme, P. Delarue, A. Bouscayrol, and P. Barrade, "La REM, formalisme multiphysique de commande de systèmes énergétiques," *Techniques de l'ingénieur, conversion de l'énergie électrique*, no. D3066, Nov. 2014. DOI: 10.51257/a-v1-d3066.

[12] D. Christen and J. Biela, "Analytical Switching Loss Modeling Based on Datasheet Parameters for mosfets in a Half-Bridge," *IEEE Transactions on Power Electronics*, vol. 34, no. 4, pp. 3700–3710, Apr. 2019. DOI: 10.1109/TPEL.2018.2851068.